Open access • Journal Article • DOI:10.1179/POM.1972.15.30.012

Dimensional and microstructural analysis of coextruded uo2-stainless steel cermet pins* — Source link

S. Nazaré, G. Ondracek, F. Thümmler

Published on: 01 Jan 1972 - Powder Metallurgy (Taylor & Francis)

Topics: Cermet, Cladding (metalworking) and Ultimate tensile strength

KERNFORSCHUNGSZENTRUM

KARLSRUHE

November 1972 KFK 1677

Institut für Material und Festkörperforschung

Dimensional and Microstructural Analysis of Coextruded UO_2-Stainless Steel Cermet Pins

S. Nazare, G. Ondracek, F. Thümmler

GESELLSCHAFT FÜR KERNFORSCHUNG M.B.H

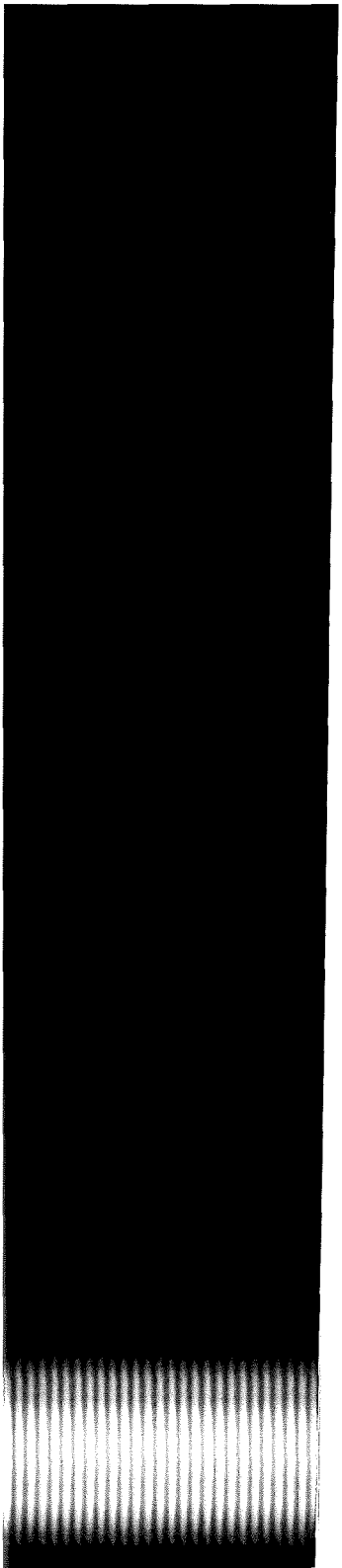

DIMENSIONAL AND MICROSTRUCTURAL ANALYSIS OF COEXTRUDED UO_2–STAINLESS STEEL CERMET PINS*

S. Nazaré,† G. Ondracek,† and F. Thümmler†

Coextrusion has been used to prepare UO_2 (35 vol.-%)–stainless steel cermet fuel-pins (5·6 mm dia. × 1000 mm long), which could be used as fuel elements in fast-flux test reactors. The procedure required to obtain a nearly homogeneous distribution of the fissile phase in the matrix is described. The influence of billet design on the dimensions of the fuel core and cladding is analysed with a view to its optimization. The extent of particle deformation as a function of extrusion parameters has been measured quantitatively by means of image analysis on particles having different (12·7%; 5·8%) inner porosities. Thermal expansion and conductivity as well as tensile strength of the cermets are reported and compared with existing data.

THE development of advanced versions of the fast-breeder reactor will require extensive testing of fuel elements and components in a fast-neutron flux. Such fast-flux test reactors will operate under conditions far more severe than those encountered in present thermal-test reactors. The neutron flux will be in the region of 10^{16}n/cm^2 s, with surface temperatures of the proposed liquid sodium coolant around 450–500°C. As a result, exacting demands will be made on the performance of the fuel element. A cermet with a greater thermal conductivity than the conventional $(UPu)O_2$ ceramic fuel would provide a very high flux by lowering the maximum operational centreline temperature of the core. The extensive and encouraging irradiation experience with UO_2–stainless steel cermets in thermal-flux environments[1] has made them obvious candidates for use in fast test reactors. They exhibit good compatibility between the components as well as with liquid sodium. However, the lower thermal conductivity of the stainless-steel matrix compared with other refractory metals, such as chromium or vanadium, is a disadvantage.

The design concept of such test reactors calls for the use of thin

* Manuscript received 1 May 1972. Contribution to a Symposium on 'The Dimensional Control of Powder Metallurgy Parts' to be held in Eastbourne on 22 November 1972.

† Institut für Material- und Festkörperforchung Kernforschungszentrum, Karlsruhe, Germany.

fuel-pins (~5·6 mm dia.), integrally clad and bonded with the stainless-steel cladding (0·3 mm thick). Among the various fabrication methods, such as swaging or hot isostatic pressing, coextrusion of powder mixtures is probably the most simple and straightforward. The object of this paper is to outline the use of coextrusion to prepare fuel-pins (35 vol.-% UO_2–stainless steel) having the following dimensions:

Pin: 5·6 mm dia. × 1000 mm long.
Fuel: 5 mm dia. × 900 mm long.

The fabrication methods developed could, at a later stage, be modified to prepare fuel-pins of PuO_2 with a stainless-steel or chromium matrix and stainless-steel cladding. Furthermore, the technique could be applied in the powder-metallurgical processing of composites to extremely small dimensions.

Choice of Powders and Materials

The concept of a dispersion fuel requires that under irradiation the zones of fission-fragment recoil (recoil zones)[2,3] do not overlap. Thus, a continuous network of undamaged matrix material is available for the dissipation and transport of fission heat. The microstructure of the cermet should therefore consist of an array of mutually supporting metallic pressure vessels, each of which retains the fission products of the enclosed ceramic particle. From the known[4] thickness of the recoil zone in stainless steel (6·7 μm), and assuming a cubic packing of spherical particles, these requirements are met only when the UO_2 particle size in the cermet (35 vol.-% UO_2) does not fall below 47 μm. Larger particle sizes (see Table I) are considered to be advantageous for the following reasons:

(1) The amount of the fission fragments recoiling in the matrix decreases with particle size.[5]
(2) For a given ceramic concentration, with increasing particle size, the network of matrix material is thicker and therefore stronger.

The upper limit is given by fabrication parameters to avoid cracking and by the temperature gradient within the UO_2 particles, which should not exceed the critical temperature (~1300–1500°C) for fission-gas release.[6] The particle size chosen on the basis of these considerations can be seen in Table I(*b*). Spherical powders were used because they have the lowest surface : volume ratio. As a result the extent of fission-fragment recoil is reduced.[7] Furthermore, the spherical shape has the lowest stress-concentration factor and thus the degradation of the mechanical properties of the matrix is reduced.[8,9]

The inner porosity of the UO_2 particles (94·2 and 87·3% TD) varied. This porosity is known to act as a reservoir for the fission products with respect to fuel swelling. Provided the matrix and cladding material exercise the needed restraint, porosity can accommodate swelling and reduce the overall dimensional changes during irradiation.[8,10,11]

The particle shape and size of the stainless-steel powder were chosen primarily on the basis of technological considerations. Too-fine particles tend to segregate during blending, and a spherical shape adversely affects the mechanical stability of the compacted cermets owing to reduced particle interlocking. The characteristics of the powders used, together with the chemical composition of the wrought stainless-steel cladding material, are shown in Tables I(*a*) and (*b*).

TABLE I(*a*). **Chemical Composition (wt.-%) of Starting Materials**

Element	Stainless-Steel Powder	Stainless-Steel Cladding
C	0·016	0·043
O_2	0·25	—
Ni	9·58	11·91
Cr	18·26	18·88
Si	0·7	0·54
Mn	0·14	1·89
Co	0·024	—
S	0·011	0·020
P	< 0·01	0·042
Fe	Bal.	Bal.

Blending of the Components

Proper blending of the components is vital for the achievement of homogeneity in the fuel core. This in turn prevents local hot spots, which can lead to premature failure in operation.

As a result of differences in density (UO_2 = 10·96 g/cm^3; stainless steel = 7·6 g/cm^3) and particle size of the components as well as the spherical shape of the UO_2 particles, considerable segregation and clustering take place when dry-blending procedures are used (tumbler movement, 70 rev/min, 1 h). This problem is especially acute during the filling of the can for the compacting operation. The microstructure of a dry-

TABLE I(*b*). **Particle Characteristics of Starting Materials**

O/U Ratio < 2·005	UO_2 87·3 TD	UO_2 94·2% TD	Stainless-Steel Powder
Particle-Size Distribution	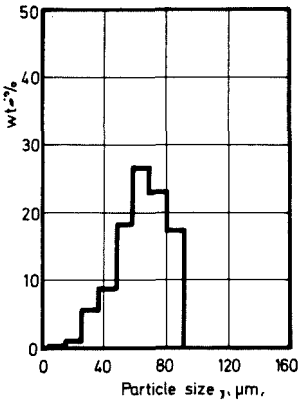	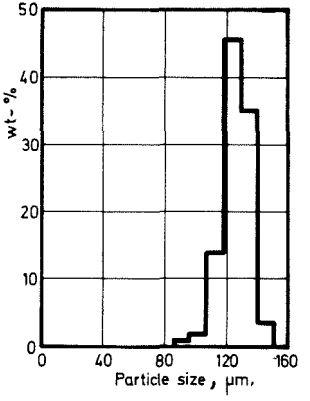	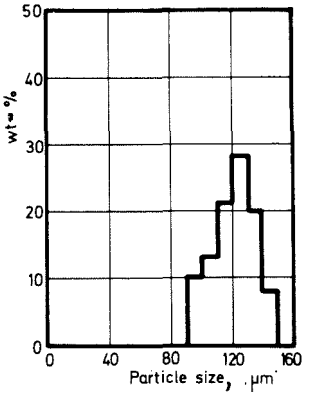
Particle Shape (Scale 1 cm = 200 μm)	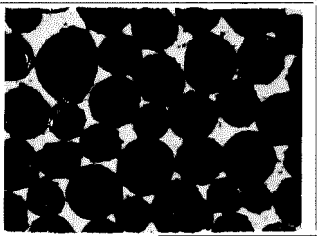	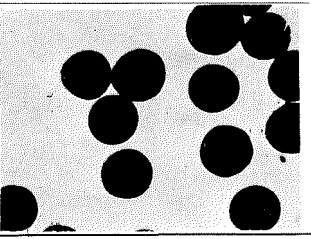	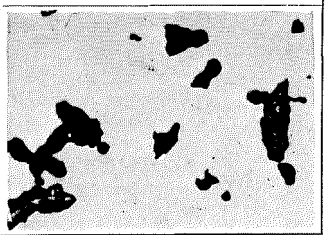

blended cermet after compaction and sintering is shown in Fig. 1(*a*). To assess the degree of distribution the microstructure of various pellets was examined with an image analyser. Fig. 1(*b*) is a plot of the concentration of UO_2 phase in a longitudinal section of a typical sample.

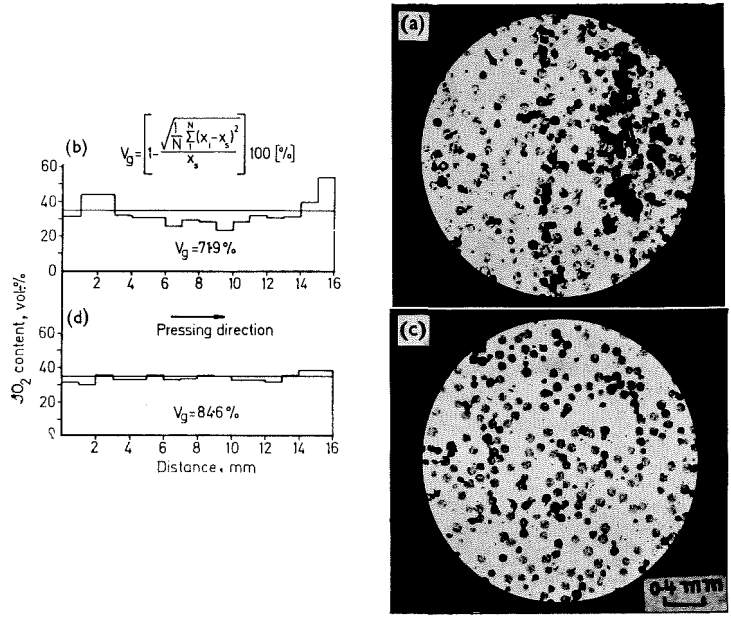

FIG. 1. Microstructure and distribution of sintered UO_2–stainless steel pellets after dry and wet blending.

The values plotted represent the mean value of five measurements at each step within an area $1 \times 1{\cdot}5$ mm. This area corresponds to ~ 25 times the area a single UO_2 particle and the corresponding matrix would occupy at the nominal concentration (35 vol.-%). The large fluctuations in concentration, especially at the bottom of the pellet, reflect the segregation occurring during die filling and compaction. To compare the results of different blending procedures, a degree of distribution may be defined using the variational coefficient of statistics:

$$V_g = \left\{1 - \sqrt{\frac{1}{N}\sum_{i=1}^{i=n}\left(1 - \frac{x_i}{x_s}\right)^2}\right\} \cdot 100(\%)$$

where

V_g = degree of distribution
x_i = ratio of the measured local volume concentration of the dispersed phase to the matrix
x_s = ratio of the known nominal volume concentration of the dispersed phase to the matrix
N = number of measurements.

The mean degree of distribution attained by dry blending (71·9%) is of course dependent on the area within which each measurement was carried out.

The unsatisfactory degree of distribution may be improved by coating the UO_2 particles with a film of stearic acid (0·5 wt.-%). The particles are then sieved on to a tray containing the stainless-steel powder and the mixture is blended by tumbler movement (70 rev/min, 1 h). The microstructure of cermets after compacting and sintering is shown in Fig. 1(*c*). The corresponding linear scan of the concentration shows a far more uniform distribution of the dispersed phase (Fig. 1(*d*)), and as a result a higher degree of distribution (84·6%). This wet-blending procedure was therefore adopted for all further experiments.

Coextrusion of Billets

The scheme for the coextrusion of the blended powder mixtures with the canning material, shown in Fig. 2, involves the following steps:

(*a*) Compaction of the mixtures in the stainless-steel can (55% TD).
(*b*) Degassing (400°C, 1·33 N/m^2 (10^{-2} torr), 2 h).
(*c*) Vacuum electron-beam welding of the end plugs.
(*d*) Jacketing of the billet in a mild-steel can. A thin film of an Al_2O_3 slurry was applied to the surface of the stainless-steel can to avoid diffusion bonding with the mild steel.

Extrusion was carried out on a horizontal hydraulic press (3·44 MN (350 Mp)). The container temperature was kept constant (450°C), the billet temperature being varied (1000–1250°C). The half-angle of the die was 45°, the front end of the billet being shaped for this angle. Graphite in oil was used as a lubricant. The ram speed varied slightly (66–76 mm/s). After extrusion the outer mild-steel sheath was removed chemically by dissolution in a bath of nitric acid. Fig. 3 shows a macroscopic view of the fuel-pins together with representative microstructures.

The recorded extrusion pressure was used to determine the extrusion constant, using the well-known relation[12]

$$P = K \ln R$$

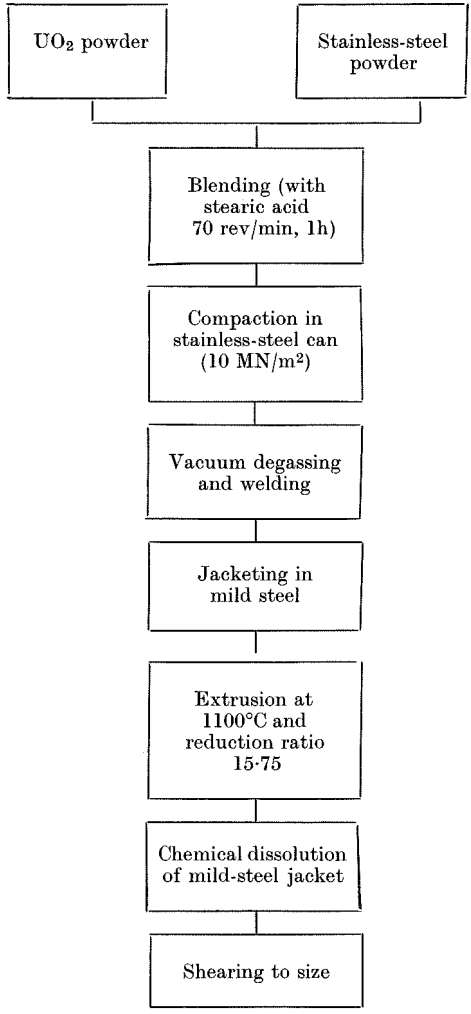

FIG. 2. Scheme adopted for the coextrusion of clad UO_2–stainless steel fuel-pins

where P = extrusion pressure
K = extrusion constant
R = reduction ratio

The extrusion constant thus obtained, which is a measure of the deformation resistance during coextrusion,[13] decreases, as expected,

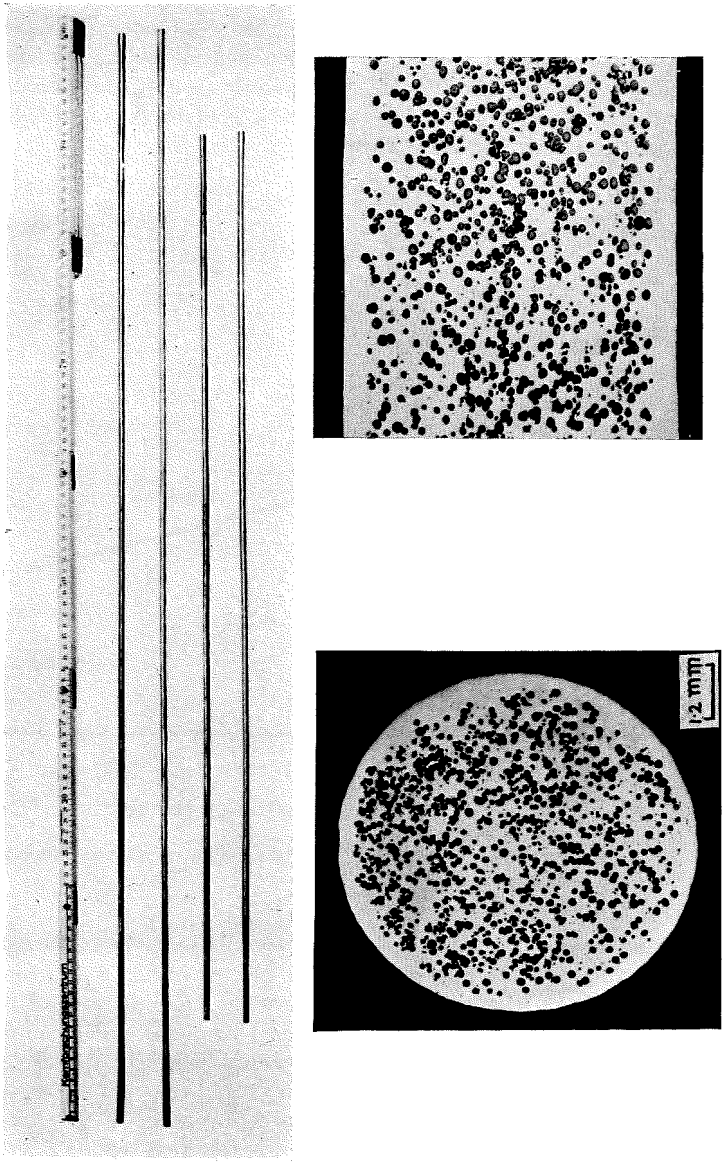

FIG. 3. View of fuel-pins prepared by coextrusion and their microstructure.

with increasing temperature (Fig. 4). It is also in agreement (Fig. 5) with known data,[14] though owing to the use of an outer mild-steel jacket the experimental conditions differed considerably. The fact that the extrusion constant does not differ greatly ($\leqslant 25\%$) from that of stainless steel explains why no defects (breaks, voids) were observed in the fuel-pins and the material coextruded easily.

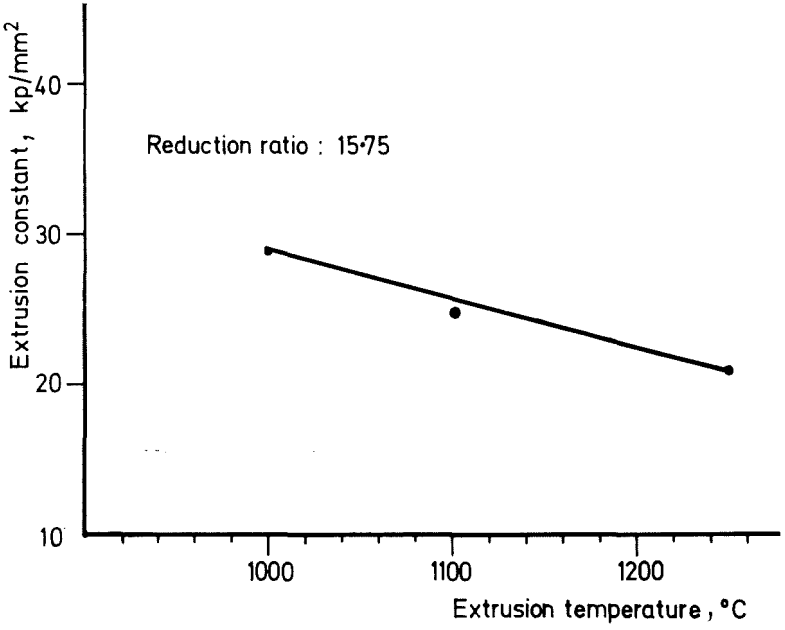

FIG. 4. Extrusion constant of UO_2 (35 vol.-%)–stainless steel cermet as a function of temperature.

The dimensions of the fuel-pins were measured along the fuel length using a microscope with cross-wires and are plotted in Fig. 6 as a function of the fuel-pin length. Also shown are the cross-sections of the stainless-steel can as well as the type of end plugs used. The can design in Fig. 6(*a*) was chosen with a view to compensating material flow during extrusion. The geometry of the front and rear plugs was designed so as to avoid the well-known effects of 'tapering' of the core in front and 'fishtailing' in the rear.[15,16] A tapered cross-section for the can was therefore used to ensure a uniform thickness of cladding along the length.

Evaluation of these initial experiments (Fig. 6(*b*)) showed that under

these experimental conditions flow was restricted to the outer mild-steel can. As a result, the cladding thickness varied almost linearly along the length, depending only on the cross-section of the can and the reduction ratio. The overall core and cladding dimensions differed, however, from those expected (5·0; 0·3 mm). This is due to the fact that before coextrusion the porous core material densifies to a point

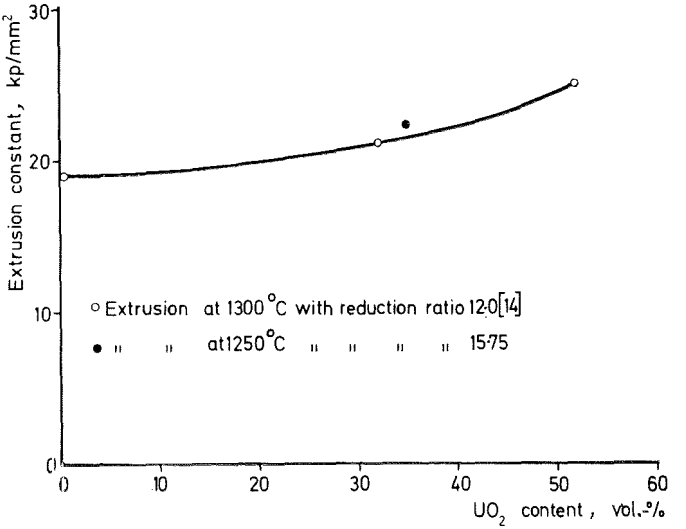

Fig. 5. Extrusion constant as a function of UO_2 content.

where its deformation-resistance corresponds to that of the solid can or end plugs. The densification involves radial as well as axial shrinkage of the porous core, with corresponding thickening of the dense can. As a consequence the final dimensions of the core are smaller than envisaged, the cladding dimensions being larger.

Calculations of the final dimensions based on fuel densification before coextrusion agreed reasonably well with the measurements (Fig. 6(*b*)). They were used as the basis for the design of the cans in Fig. 6(*c*) and 6(*e*). The dimensions of the fuel-pins (Fig. 6(*d*)) show that close tolerances can be attained in the core region. Since the solid end plugs do not densify before coextrusion, thickening of the fuel-pin end occurs at the front and rear. This can be overcome by using porous (55% TD) plugs of stainless steel, thus ensuring uniformity of dimensions along the whole fuel-pin (Fig. 6(*e*)).

Radiographs of the fuel-pins showed that the extent of end defects

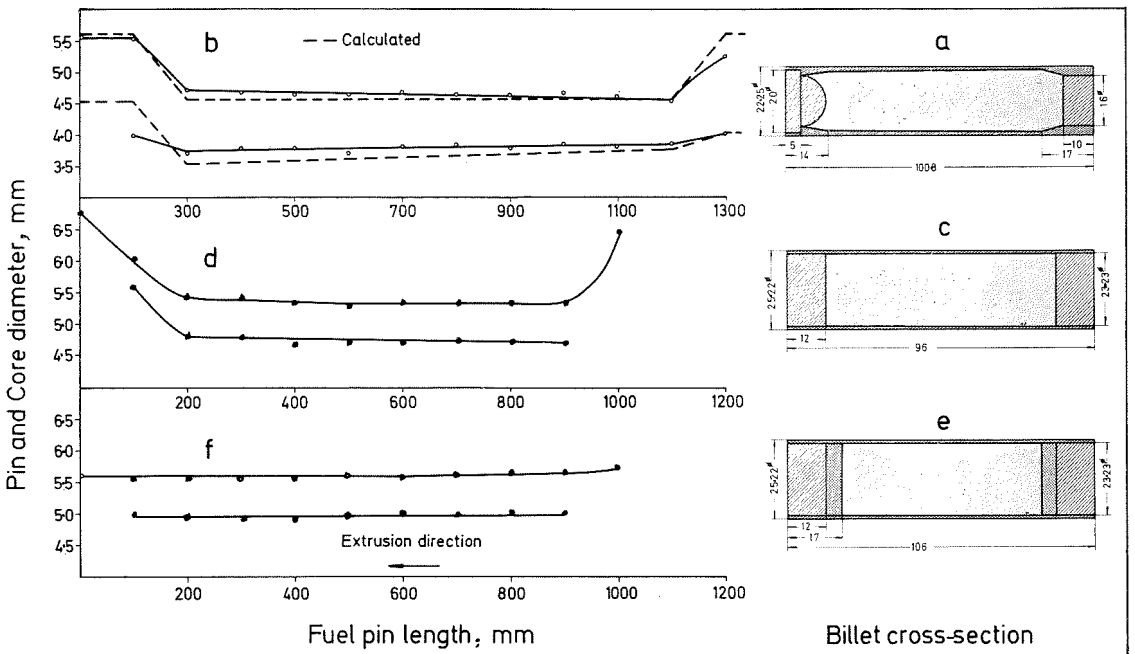

FIG. 6. Dimensions of coextruded UO_2–stainless steel fuel-pins with various billet designs.

was restricted to a small zone (10 mm) at each end. Further tests included the distribution of the UO_2 phase in the fuel-pin by the method described previously. Plotted in Fig. 7 is a scan of the UO_2 concentration along the fuel-element length. The degree of distribution obtained (84%) as well as the representative microstructure show that the homogeneity of the dispersions is not appreciably altered during extrusion (see Figs. 1(*c*) and 1(*d*)). However, some slight geometrical effects are apparent. The particle shape is considerably changed during

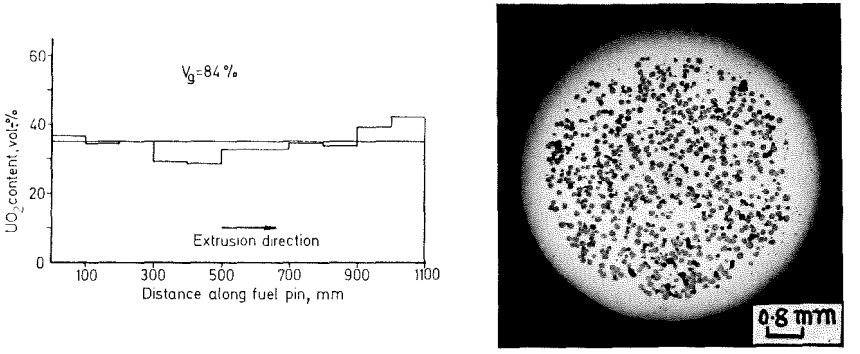

FIG. 7. Distribution of UO_2 in coextruded UO_2–stainless steel fuel-pins.

extrusion. In this respect the extrusion parameters can be optimized to reduce particle stringering, so that the desirable spherical shape is not very much changed in the finished fuel-pin. With this aim in view a microstructural analysis of the fuel-pins with varying extrusion parameters was carried out. The texture was chosen as a measure of the stringering and defined as

$$Y = \frac{p_x}{p_y}$$

where Y = texture factor.

p_x = projected length of UO_2 particles in the extrusion direction.

p_y = projected length of UO_2 particles at right angles to the extrusion direction.

The measurements were carried out with an image analyser at various points in the fuel-pins. In Fig. 8(*a*) the texture factor is plotted along the fuel-pin length for two extrusion temperatures. It can be seen that a higher extrusion temperature reduces stringering since the lower deformation-resistance of the matrix decreases the compressive stresses

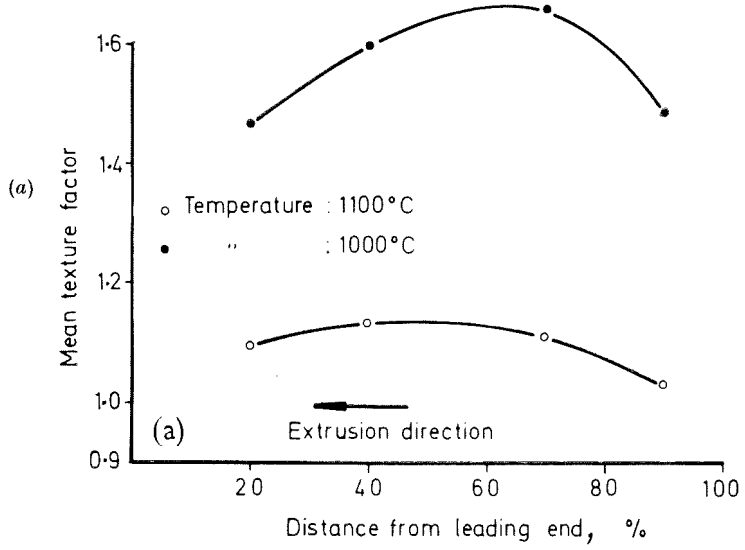
(a)
Mean texture factor
1·6
1·4
1·2
1·0
0·9
o Temperature : 1100°C
• " : 1000°C
(a)
Extrusion direction
20
40
60
80
100
Distance from leading end, %

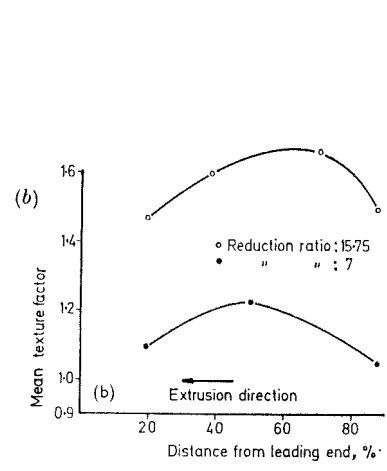
(b)
Mean texture factor
1·6
1·4
1·2
1·0
0·9
o Reduction ratio: 15·75
• " " : 7
(b)
Extrusion direction
20
40
60
80
Distance from leading end, %

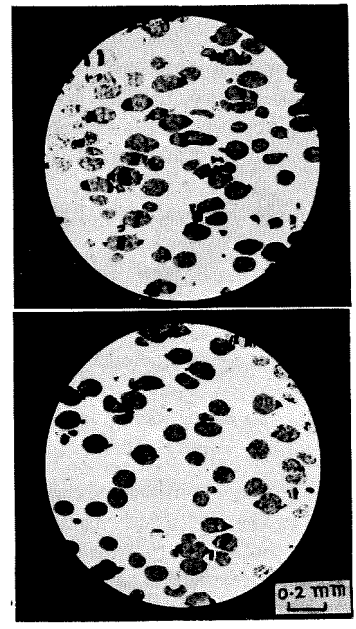
0·2 mm

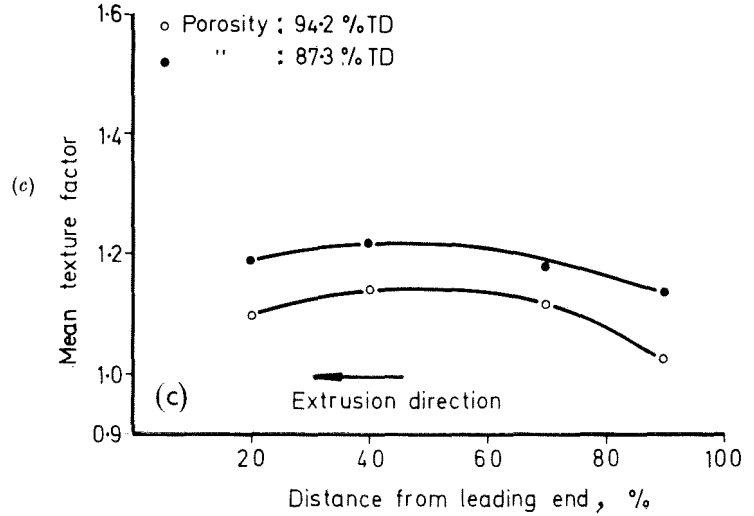

FIG. 8(*a*). Texture factor of UO_2 (94·2% TD) along the fuel-pin at different extrusion temperatures (reduction ratio 15·75).
(*b*). Texture factor of UO_2 (94·2% TD) along the fuel-pin at various reduction ratios (extrusion temperature 1000°C).
(*c*). Texture factor of UO_2 along fuel-pins of varying porosity (extrusion temperature: 1100°C, reduction ratio 15·75).

induced in the UO_2 particles. These results are similar to those obtained during rolling of UO_2–stainless steel fuel-plates.[17–20] The lower deformation of the UO_2 particles at the ends of the fuel-pin is probably caused by the fact that during densification before coextrusion the particles are slightly deformed at right angles to the extrusion direction. This predeformation is apparently greater at the ends than in the centre. During subsequent extrusion, the particles are again deformed—this time in the extrusion direction. The result of these opposing effects leads to the final stringering in the fuel core, with the maximum texture in the central region.

The effect of the reduction ratio on stringering can be seen in Fig. 8(*b*). Obviously a large reduction ratio leads to increased stringering, which is also apparent in the representative microstructures of the pin. However, it promotes good metallurgical bonding between the fuel and the cladding and does not lead to unduly small dimensions of the can before extrusion.

Finally, in Fig. 8(*c*) the influence of the porosity of the UO_2 particles on stringering can be seen. It seems that provided the strength of the

UO_2 particles does not fall below certain limits the porosity does not greatly affect the deformation of the particles during extrusion. At the chosen extrusion temperature (1100°C) and reduction ratio (15·75) the fragmentation of the porous UO_2 particles (94·2 and 87·3% TD) was minimal.

Properties of UO_2–Stainless Steel Cermets

A fairly large amount of data is already available on those properties of UO_2–stainless steel cermets that are of importance for reactor use.[21-23] The measurements outlined below were therefore carried out primarily to ascertain the influence of the inner porosity of the UO_2 particles on properties. All the measurements were carried out on extruded samples of a high matrix density (99·7%TD) after removal of the cladding material.

Thermal Expansion

Thermal expansion was measured in vacuum ($< 1{\cdot}33 \times 10^{-2}$ N/m^2, $< 10^{-4}$ torr) using a push-rod dilatometer calibrated with a gold standard. Fig. 9 shows the mean linear thermal expansion coefficient (20–900°C)

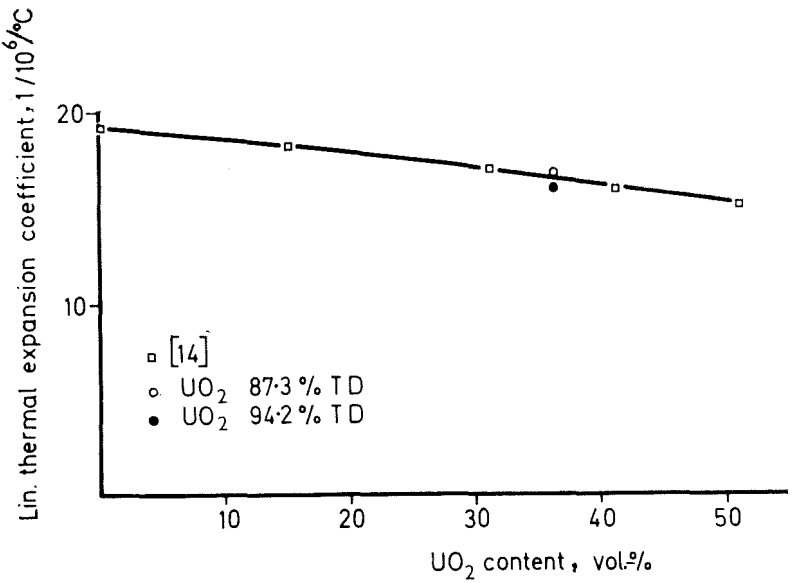

FIG. 9. Linear thermal expansion coefficient (20–900°C) of UO_2– stainless steel cermets as a function of UO_2 concentration.

as a function of UO_2 concentration. It can be seen that, within the limits of experimental accuracy, thermal expansion is not dependent on the inner porosity but only on the volume concentration of the dispersed phase. This is to be expected, since the thermal expansion of the cermet results from the expansion of the matrix and mechanical restraint caused by the expansion of the included phase.[24] However, since porosity does not affect the thermal expansion of the included phase,[25] its influence on the expansion of the cermet remains unchanged. The data are, as can be seen, in good agreement with known results.

Thermal Conductivity

The measurements were carried out with a special longitudinal heat-flow apparatus[26] at 93·5°C and are compared in Fig. 10 with known results[14] obtained at 600°C. This comparison is justifiable, since the thermal conductivity of these cermets is only slightly affected by temperature.[24] The measurements for both ranges of porosity lie within experimental accuracy. They are in agreement with theoretical predictions, which show that for the small change in porosity involved the variation of thermal conductivity in the low-temperature range should be indeed small.

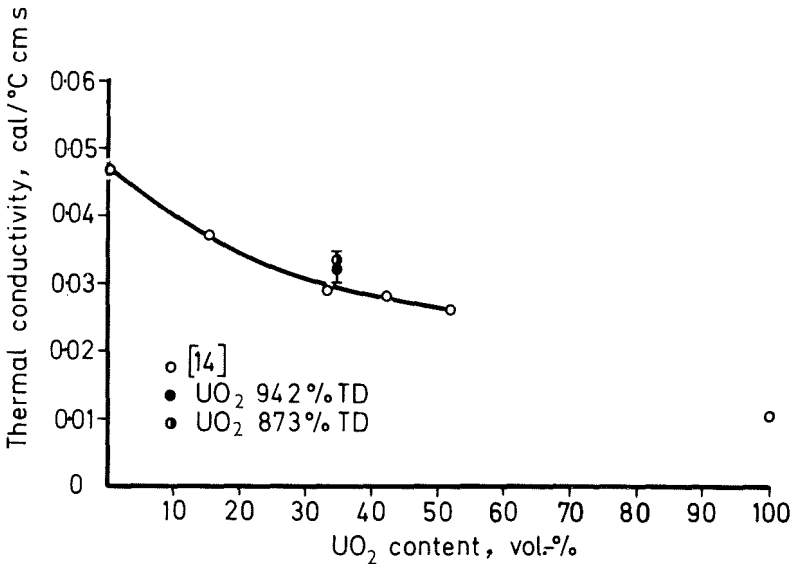

FIG. 10. Thermal conductivity as a function of UO_2 concentration.

Tensile Strength

The tensile strength, measured at various temperatures in an inert (argon) atmosphere, is plotted in Fig. 11 as a function of temperature. It was found that inner porosity did not influence the strength. This is in agreement with various known results,[21,22,27] which show that the strength of the cermet is dependent only on the load-bearing area of the matrix, when the interfacial bonding is weak.

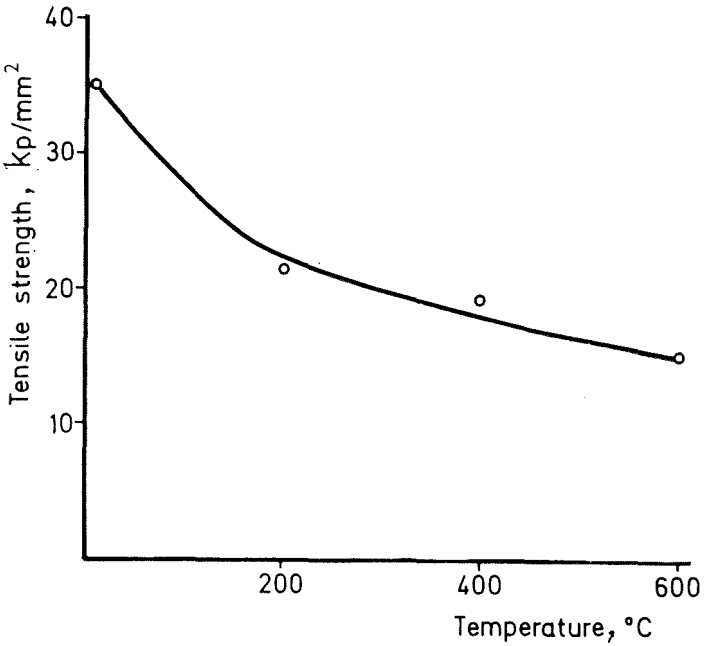

FIG. 11. Tensile strength of UO_2 (35 vol.-%)–stainless steel cermets as a function of temperature.

Conclusions

(1) A nearly homogeneous distribution of the UO_2 phase can be obtained by coating the UO_2 particles with stearic acid before blending.

(2) Thin fuel-pins with close and uniform dimensions can be prepared by coextrusion of powder mixtures. The use of porous front and rear plugs ensures satisfactory dimensional control of the end seals.

(3) A higher extrusion temperature is advantageous in reducing the degree of particle deformation.

(4) Thermal expansion, conductivity, and tensile strength are not greatly affected by the inner porosity of the UO_2 particles in the range of porosity used in the experiments.

Acknowledgements

The authors thank Dr. Ruehle of Metallgesellschaft, Frankfurt, for his cooperation in extrusion experiments and Mr. J. Buerkin for experimental assistance.

References

1. W. C. Thurber, *US Atomic Energy Commission Rep.* (**ORNL-3709**), 1964.
2. A. N. Holden, 'Dispersion Fuel Elements'. **1968**: New York (Gordon and Breach).
3. D. W. White *et al.*, *US Atomic Energy Commission Rep.* (**TID-7546**), Book 2, 1957.
4. D. L. Keller, *Nucleonics*, 1961, **19**, 45.
5. C. E. Weber, cited in 'Progress in Nuclear Energy', Series V 'Metallurgy and Fuels'. **1959**: New York and London (McGraw-Hill).
6. M. B. Waldron, *Powder Met.*, 1967, **10**, 288.
7. G. E. Goslee, *Nucleonics*, 1963, **21**, 48.
8. J. R. Weir, *US Atomic Energy Commission Rep.* (**ORNL-2902**), 1960.
9. J. E. Cunningham, *ibid.*, (**ORNL-P-2355**), 1964.
10. M. J. Graber *et al.*, *ibid.*, (**IN-1160**), 1968.
11. G. W. Gibson, *ibid.*, (**IN-1131**), 1967.
12. C. E. Pearson and B. N. Parkins, 'The Extrusion of Metals'. **1961**: London (Chapman and Hall).
13. P. Lowenstein, cited in 'Nuclear Reactor Fuel Elements' (edited by A. R. Kaufmann). **1962**: New York (Interscience Publishers).
14. L. Meny, J. Buffet and Ch. Sauve, 'Powder Metallurgy in the Nuclear Age' (4th Plansee Seminar), p. 566. **1962**: Reutte/Tyrol (Metallwerke Plansee).
15. H. Steinkopf and L. Löffler, *Kernenergie*, 1963, **6**, 315.
16. K. Ennerst et al., *Atomwirtschaft*, 1963, **3**, 325.
17. A. J. Taylor, *US Atomic Energy Commission Rep.* (**ORNL-3645**), 1964.
18. J. H. Cherubini and S. A. Rabin, *ibid.*, (**ORNL-3160**), 1961.
19. D. E. Lozier and D. E. Kizer, *ibid.*, (**BMI-X-10172**), 1966.
20. R. W. Dayton, *ibid.*, (**BMI-1697**), 1964.
21. S. Nazaré and G. Ondracek, *Atomkernenergie*, 1971, **17**, 251.
22. L. H Cope, *Metallurgia*, 1965, **72**, 165.
23. G. Arthur and J. A. Coulson, *J. Nuclear Mat.*, 1964, **13**, 242.
24. S. Nazaré and G. Ondracek, 'Proceedings of the European Conference on Thermophysical Properties 1970' p. 631, **1970**: Bonn (Bundesministerium für Bildung und Wissenschaft).
25. R. L. Coble and W. D. Kingery, *J. Amer. Ceram. Soc.*, 1956, **39**, 377.
26. J. Schröder, *Rev. Sci. Instruments*, 1963, **34**, 615.
27. G. D. MacAdam, *Powder Met.*, 1967, **10**, 307.